PAPER

Check for updates

Enhancing waste eggshell-derived CaO catalysts for biodiesel production through synergistic oxide modification: a comprehensive catalytic and kinetic study

Lebohang Macheli, [iD] *[a] Gerard M. Leteba, [iD] [b] Sarah L. George,[b] Candace I. Lang[b] and Linda L. Jewell*[a]

Valorizing waste materials for sustainable biodiesel production offers dual benefits of environmental remediation and cost reduction. In this study, calcium oxide (CaO) derived from waste eggshells was modified with metal oxides—SiO_2, TiO_2, and Co_2SiO_4—to overcome limitations of pure CaO catalysts, such as leaching, low surface area, and reduced reusability. The catalysts were synthesized *via* wet impregnation followed by calcination, and their physicochemical properties were systematically correlated with transesterification performance under identical optimized reaction conditions, enabling direct structure–activity comparison. Among the modified catalysts, TiO_2-modified CaO exhibited the highest FAME yield (89.7%) due to synergistic effects that enhanced basicity (1.103 mmol g^{-1}) and surface area (121.9 m^2 g^{-1}), supported by XRD data of $CaTiO_3$ phase formation. Detailed kinetic analysis confirmed pseudo-first-order behavior, and equilibrium data for all catalysts collapsed onto a single Hill isotherm, revealing cooperative adsorption effects that appear intrinsic to the transesterification equilibrium rather than catalyst specific. Apparent turnover frequency (TOF) analysis, normalized by basic site concentration, showed broadly comparable per-site activity across the catalyst series, with CaO–SiO_2 giving the highest operational TOF, indicating improved site accessibility rather than intrinsically faster kinetics. The modified catalysts demonstrated minimal deactivation (<2% loss over four cycles), attributed to oxide-induced stabilization of CaO active sites. This work provides new mechanistic insight into cooperative adsorption and site utilization in waste-derived CaO catalysts, advancing the rational design of durable heterogeneous catalysts for biodiesel synthesis.

1. Introduction

The environmental and ethical challenges posed by fossil fuels and first-generation biodiesel feedstocks necessitate the exploration of sustainable alternatives such as biofuels.[1–3] Biodiesel, a renewable and eco-friendly diesel substitute, offers a high flash point, cetane number, lubricity, non-toxicity, and low sulfur content, making it a viable replacement for conventional diesel.[4,5] While first-generation biodiesel production relies on edible oils, second-generation feedstocks such as waste cooking oil (WCO) avoid competition with food resources and help mitigate environmental pollution.[3,6–8] Valorizing WCO not only reduces disposal-related hazards but also lowers biodiesel production costs,[9–13] although its complex and variable composition presents challenges for catalyst performance

evaluation and kinetic interpretation, as also observed in biodiesel systems employing waste-derived alkali-rich heterogeneous catalysts.[14,15]

Heterogeneous catalysts, particularly calcium oxide (CaO) derived from waste eggshells, have received significant attention for biodiesel synthesis due to their low cost, environmental friendliness, ease of separation, and potential for reuse.[13] However, unmodified CaO suffers from limitations such as leaching of active species, surface carbonation, relatively low surface area, and gradual deactivation upon reuse.[16] Addressing these shortcomings through surface and structural modification is key to improving both catalytic activity and stability. Notably, many reported CaO-based studies focus on single modifiers and are often evaluated under different reaction conditions, limiting direct comparison and clear understanding of modifier-specific structure–performance relationships.[17,18]

Metal oxide modification of CaO is a proven strategy for tuning its physicochemical properties.[16] In this work, we present a systematic comparative study of waste eggshell-derived CaO modified with three different oxides—SiO_2, TiO_2,

[a]Department of Chemical and Materials Engineering, University of South Africa, Cnr Christian De Wet and Pioneer Road, Florida 1709, Johannesburg, South Africa. E-mail: machelg@unisa.ac.za; jewelll@unisa.ac.za

[b]Centre for Materials Engineering, Department of Mechanical Engineering, University of Cape Town, P/Bag X3 Rondebosch 7708, Cape Town, South Africa

and Co_2SiO_4—chosen for complementary reasons and evaluated under identical reaction conditions with unmodified CaO serving as a baseline catalyst. SiO_2 is well known for improving dispersion and increasing surface area, potentially enhancing reactant–catalyst contact.[19,20] TiO_2 can strongly interact with CaO to form mixed oxides such as $CaTiO_3$ (ref. 21 and 22) which have been reported to boost basicity and structural stability.[17] Co_2SiO_4, to the best of our knowledge, is applied here for the first time in biodiesel catalysis, addressing a clear gap in CaO-based catalyst modification strategies; its robust orthosilicate structure and potential to stabilize CaO active sites present an unexplored opportunity for improving catalyst durability. By comparing these modifiers under identical conditions, this study identifies not only the best-performing system but also the distinct property–performance relationships for each oxide.

Beyond yield measurements, we incorporate a Hill isotherm model to describe equilibrium behavior in the trans-esterification process. Cooperative adsorption phenomena, as indicated by the model, are rarely investigated in biodiesel catalysis despite their potential to inform active site engineering,[23] and kinetic interpretations in this study are treated on a comparative basis to account for the inherent complexity of WCO feedstocks. Additionally, catalyst stability is evaluated over multiple reaction cycles, providing practical insights into long-term performance—an aspect often underreported in waste-derived catalyst studies.[7,24,25] Overall, this work aims to deliver a clear understanding of how targeted oxide modification impacts the surface chemistry, basicity, and durability of CaO-based catalysts for WCO transesterification, bridging sustainable catalyst design with applied biodiesel production.

2. Materials and methods

2.1. Materials

All chemicals were purchased from Merck Chemicals (Pty) Ltd unless otherwise stated. Waste eggshells were collected locally, rinsed with water to remove surface debris and proteins, and dried before processing. Waste cooking oil (WCO) was sourced from a local restaurant, filtered to remove food residues, and dehydrated by heating at 378 K for 60 min to remove residual moisture. Methanol ($\geq$99.8%) was used as the alcohol source for transesterification.

2.1.1. Synthesis of CaO. Cleaned eggshells were treated with 0.25 M sulfuric acid to remove residual organics, then rinsed thoroughly with hot distilled water. The shells were dried, ground to a particle size <200 μm, and calcined in air at 1173 K for 2 h to produce CaO. The calcined CaO was stored in a desiccator to minimize surface carbonation before use.

2.1.2. Preparation of the oxide. Silica (SiO_2) was purchased from Merck Chemicals and used without further modification. Titanium dioxide (TiO_2, P25; Evonik) with an anatase/rutile mixed phase was used as received. Cobalt orthosilicate (Co_2SiO_4) was synthesized by co-precipitating silicic acid and cobalt nitrate hexahydrate at a Co:Si molar ratio of 2:1, followed by the dropwise addition of ammonium hydroxide until complete precipitation occurred. The resulting precipitate was thoroughly washed with distilled water, dried at 393 K, and calcined in air at 1273 K for 30 min to obtain a deep purple powder.

2.1.3. Modification of CaO with different oxides. Oxide-modified CaO catalysts ($CaO–SiO_2$, $CaO–TiO_2$, $CaO–Co_2SiO_4$) were prepared by dispersing <200 μm CaO powder in aqueous suspensions of the respective oxide (final composition: 75 wt% CaO, 25 wt% oxide). The mixtures were sonicated at 353 K for 60 min, dried at 393 K overnight, and calcined in air at 1173 K for 2 h. All catalysts were stored in sealed containers to prevent moisture and CO_2 uptake.

2.1.4. Catalyst characterization. Catalyst morphology was examined by transmission electron microscopy (TEM: JEM200CX, JEOL, Japan). Phase composition was determined using powder X-ray diffraction (XRD, Bruker AXS D8) with Co-Kα radiation ($\lambda = 0.178897$ nm) at 40 kV, 40 mA, and a VANTEC detector. Fourier transform infrared (FTIR) spectra were collected on a Nicolet 5700 spectrometer using KBr pellets. BET surface area was determined by N_2 adsorption at 77 K (Micromeritics ASAP 2020). Catalyst basicity was quantified by the Tanabe and Yamaguchi titration method,[26] which provides a semi-quantitative estimate of accessible basic sites. This method does not resolve basic site strength distributions and was therefore used solely for comparative analysis among catalysts synthesized and evaluated under identical conditions. Accordingly, turnover frequencies reported in this study are designated as apparent TOFs and are not intended to represent absolute site-specific kinetic constants.

2.1.5. Transesterification procedure. The transesterification reaction was carried out under reflux condensation using a 250 mL two-neck round-bottom flask equipped with a reflux condenser and a magnetic stirrer. Purified waste cooking oil (50 mL) was added to the flask and heated to the desired reaction temperature at atmospheric pressure. Methanol (MeOH) and the pre-treated catalyst—calcined at 773 K for 2 h—were subsequently introduced at the specified methanol-to-oil molar ratio. The reaction mixture was vigorously stirred at 1200 rpm using catalyst particles ground to <75 μm to ensure homogeneity and to minimize both external and internal mass transfer limitations, in accordance with recommended biodiesel testing practice.[27] While no formal mass transfer diagnostic tests (e.g., Weisz–Prater analysis or stirring-speed variation) were performed, the high agitation rate and fine particle size are consistent with literature conditions known to suppress mass transport artifacts in similar heterogeneous base-catalyzed systems. Reactions were conducted for 60 min, after which the catalyst was separated by gravitational settling (4–5 h). The resulting two-phase mixture was transferred to a separating funnel and left overnight to complete phase separation. The biodiesel phase was further purified by heating at 373 K for 10 min to remove residual methanol. All transesterification experiments were performed in triplicate unless otherwise stated. Reported fatty acid methyl ester (FAME) yield values represent the mean of three independent runs, and the associated variability is expressed as standard deviation. Error bars shown in the corresponding figures reflect standard deviation.

To determine the optimal reaction conditions, unmodified CaO was used while varying the methanol-to-oil molar ratio (4 : 1 to 14 : 1), catalyst loading (1–6% w/v), and reaction temperature (313–343 K). Unmodified CaO was selected as the baseline catalyst to establish intrinsic reaction conditions independent of oxide modification effects. The highest FAME yield was achieved at a methanol-to-oil ratio of 10 : 1, a catalyst loading of 5% (w/v), and a reaction temperature of 333 K. These optimized conditions were subsequently applied to evaluate the catalytic performance of CaO–SiO$_2$, CaO–TiO$_2$, and CaO–Co$_2$SiO$_4$. Catalyst reusability was assessed under optimized conditions. After each cycle, the catalyst was recovered by filtration, washed with *n*-hexane, dried at 393 K, and re-calcined at 773 K before reuse. Unmodified CaO maintained activity for up to four cycles, though a gradual decline was observed, whereas oxide-modified catalysts showed improved stability.

For comparative purposes, apparent turnover frequencies (TOFs) were calculated from the FAME yield after 60 min under the optimized reaction conditions. The TOF was defined as:

$$TOF = \frac{\text{moles of FAME produced}}{\text{moles of basic sites} \times \text{time}}$$

FAME yields were quantified by gas chromatography with flame ionization detection (GC-FID) using methyl nonadecanoate as an internal standard. This method enables direct determination of total FAME content and inherently accounts for variations in fatty-acid chain length and composition present in waste cooking oil. The number of basic sites was obtained from titration-derived basicity values (mmol g^{-1}) multiplied by the mass of catalyst used (5% w/v relative to the oil mass). The reaction time considered for all TOF calculations was 3600 s (60 min). Turnover frequencies (TOFs) were calculated from the GC-derived molar FAME yield obtained after 60 min under optimized reaction conditions and normalized to the total number of basic sites determined by titration. The reaction time used for all TOF calculations was 3600 s. These TOF values are designated as apparent TOFs, as they do not account for variations in basic site strength, approach to equilibrium, or potential catalyst deactivation at high conversion. Accordingly, TOF values are used to compare relative catalytic performance rather than to provide absolute site-specific kinetic constants. Given the semi-quantitative nature of titration-derived basicity values and the absence of site strength differentiation, the calculated TOFs are used to compare relative catalytic performance rather than to infer intrinsic kinetic parameters.

3. Results and discussion

The physicochemical properties of the feedstock oil and the produced biodiesel were determined according to the method of Ejim and Kamen (see Table 1).[28] Density was calculated from mass and volume measurements obtained using a high-precision balance and calibrated pipette, according to:

$$\text{Density} = \text{mass/volume}$$

The free fatty acid (FFA) content of the feedstock oil was determined by warming 4 g of oil in a 250 mL conical flask, adding two drops of phenolphthalein indicator and one drop of 0.14 M sodium hydroxide (NaOH) solution, followed by 25 mL of methanol. The mixture was vigorously shaken and titrated with 0.14 M NaOH until a persistent pink colour was observed. The endpoint volume was used to calculate the FFA value. The acid value of the biodiesel was determined using the same procedure.

3.1. Optimization of reaction conditions (unmodified CaO)

Temperature is a key factor influencing the efficiency and yield of the transesterification process. In this study, the transesterification of waste cooking oil was performed at various temperatures: 318 K, 323 K, 328 K, 333 K and 338 K, using CaO as a catalyst. The yield of biodiesel at each temperature was monitored over time, and the results are presented in Fig. 1a. The highest FAME yield of 80.3% was achieved at 333 K after 60 minutes of reaction time. Therefore, the optimal temperature for biodiesel production *via* the conventional method was determined to be 333 K. The increase in FAME yield with rising temperature up to 333 K can be attributed to the enhanced reaction rate at higher temperatures. As the temperature increases, the kinetic energy of the molecules also increases, leading to more frequent and effective collisions between reactant molecules, which in turn accelerates the transesterification process.[29] Additionally, higher temperatures can reduce the viscosity of the oil, improving the mass transfer between the reactants and the catalyst, which further enhances the reaction rate.[30] However, a decline in FAME yield was observed when the reaction temperature increased to 338 K. This decrease may be linked to the vaporization of MeOH, which occurs as the temperature approaches its boiling point (338 K). The vaporization of MeOH will mean that MeOH is the limiting reagent, leading to a decrease in the reaction rate and thus a lower biodiesel yield.[31] Moreover, excessive temperatures can lead to side reactions, such as the formation of soap, which can further reduce the biodiesel yield.[25]

The MeOH-to-oil ratio is a critical parameter in the transesterification process, as it significantly impacts the conversion efficiency and yield of biodiesel. In this study, the MeOH-to-oil ratio varied between 4 : 1 and 14 : 1 while maintaining an optimized reaction temperature of 333 K (Fig. 1b). The FAME yield increased progressively with the MeOH-to-oil ratio, peaking at the ratio of 10 : 1. Beyond this optimal ratio, a decline in yield was observed as the ratio increased. The initial increase in biodiesel yield with rising MeOH-to-oil ratios can be attributed to the law of mass action, where an excess of MeOH drives the reaction equilibrium towards the production of more biodiesel, overcoming the reversible nature of the transesterification reaction.[32,33] This is consistent with previous findings that an excess of MeOH is necessary to achieve higher conversion rates.[16] However, at ratios of 12 : 1 and 14 : 1, the yield decreases, which may be due to the dilution of reactants, reducing the effective collision frequency between oil molecules and the catalyst.[33,34] Additionally, excessive MeOH can lead to increased

Table 1 Physicochemical properties of oil and diesel synthesized using various catalyst

Physicochemical property	Measure waste cooking oil	Diesel (CaO)	Diesel (CaO–SiO$_2$)	Diesel (CaO–TiO$_2$)	Diesel (CaO–Co$_2$SiO$_4$)
Physical state (at 328 K)	Liquid	Liquid	Liquid	Liquid	Liquid
Color	Golden brown 900	Clear 887	Clear 873	Clear 882	Clear 876
Density (kg L^{-1})	—	0.53	0.59	0.48	0.65
Acid value (mg KOH per g)	1.2%	—	—	—	—
FFA content (wt%) saponification value (mg KOH per g)	167	—	—	—	—

solubility of glycerol in the MeOH phase, complicating the separation process and thereby reducing the overall biodiesel yield.[35]

The amount of catalyst used is another vital factor influencing the efficiency of the transesterification process. In this study, CaO derived from eggshells was used as a catalyst, and its loading varied between 1% and 6% (w/v). Experiments were conducted under the optimized temperature of 333 K and

a MeOH : oil ratio of 10 : 1. As the catalyst loading increased from 1% to 5% (w/v), the biodiesel yield also increased, with the highest yield observed at 5% (w/v) catalyst loading (Fig. 1c). Beyond this point, further increases in catalyst loading did not lead to any significant improvement in yield, which remained steady. The enhancement in biodiesel yield with increasing catalyst loading up to 5% (w/v) can be attributed to the greater availability of active sites on the catalyst surface, which
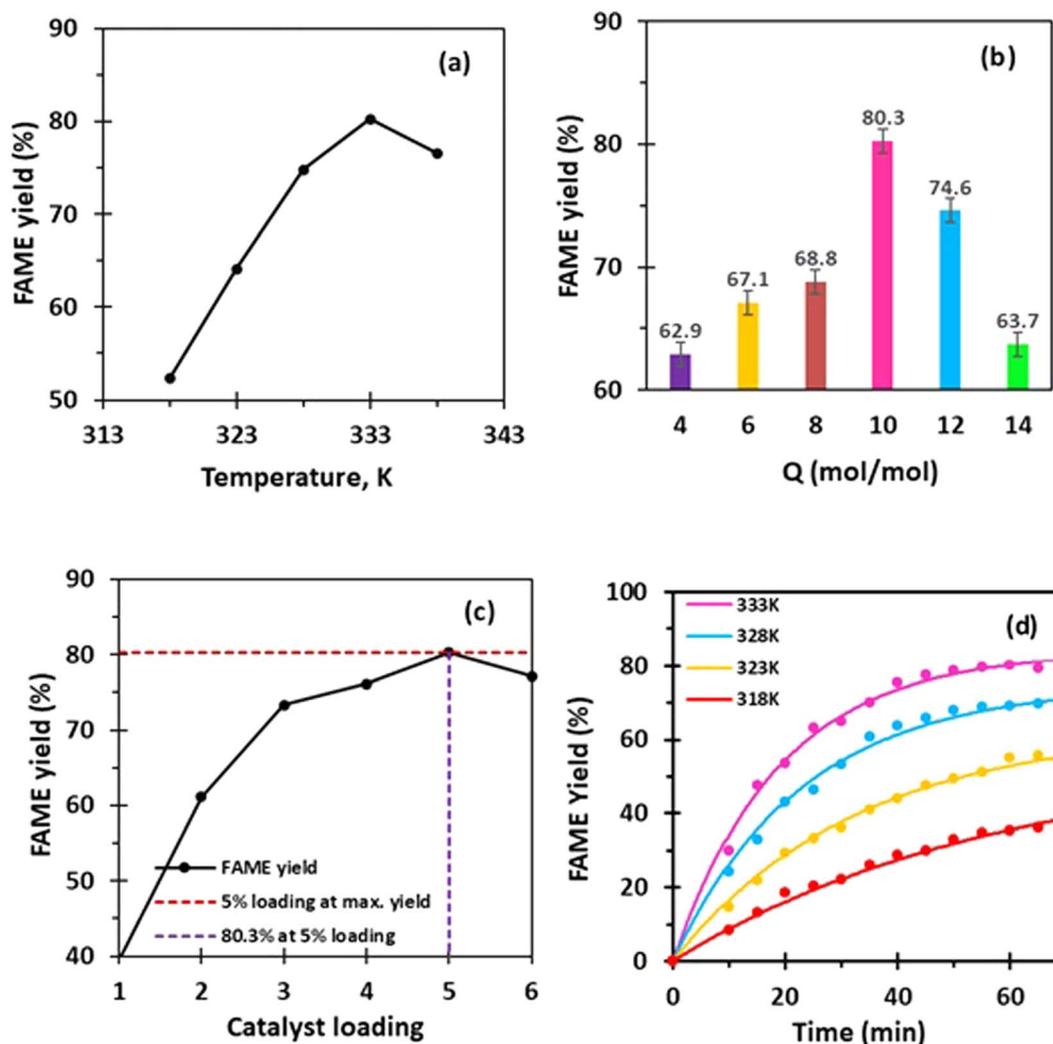

Fig. 1 Optimization of (a) transesterification reaction temperature at MeOH-to-oil ratio of 10 (catalyst loading of 5 g/100 mL), (b) using CaO at 333 K and catalyst loading of 5% (w/v), (c) FAME yield as a function of catalyst loading using unmodified CaO catalyst and (d) FAME yield as a function of time at different reaction temperature.

accelerates the reaction rate.[36] However, beyond this optimum loading, the yield does not increase further. This plateau effect may result from the change in viscosity of the reaction mixture, hindering efficient mixing and slowing mass transfer between phases.[37] Moreover, excess catalyst may increase the viscosity of the reaction mixture, leading to poor mixing and mass transfer limitations, which counteract the benefits of higher catalyst loading.[38,39]

For the optimization of reaction time, experiments were conducted at different temperatures (318 K, 323 K, 328 K, and 333 K) to determine the time required to achieve maximum FAME yield. The reaction was monitored at regular intervals, and FAME yield was plotted against time for each temperature. The conversion of oil to biodiesel exhibited a characteristic trend with time, as shown in Fig. 1d. Initially, the conversion increased rapidly due to the high availability of reactants and active catalytic sites. This trend is consistent with previous studies where the reaction follows pseudo-first-order kinetics under excess methanol conditions, particularly for biodiesel synthesis using waste-derived heterogeneous base catalysts.[14,15,40,41] At the optimized temperature of 333 K, the highest FAME yield (80.3%) was achieved within 60 minutes, after which no significant increase was observed. This observed plateau reflects the system approaching an apparent kinetic asymptote within experimental time window rather than true thermodynamic equilibrium, a phenomenon also reported by Meher et al.[42] where prolonged reaction times did not yield further improvements in the yield. Furthermore, at lower temperatures (318 K and 323 K), the formation of FAME proceeded at a slower rate, demonstrating the temperature dependence of reaction kinetics. Reaction kinetics were determined by non-linear regression of GC-measured FAME yield *versus* time using the pseudo-first-order kinetic model expressed as

$$Y = Y_{as}(1 - e^{-kt})$$

where Y is the FAME yield, Y_{as} represents the asymptotic FAME yield approached within the experimental time window, k is the apparent rate constant and t is time.[43,44] The apparent reaction rate constant increased systematically with temperature from 318 K to 333 K (Table 2). Arrhenius analysis showed that the temperature dependence was primarily reflected in an increase in the pre-exponential factor, while the activation energy remained nearly constant, indicating that the enhancement in reaction rate is mainly associated with increased effective

collision frequency and improved reactant accessibility rather than a change in the intrinsic energy barrier.[43–45] The constant activation energy across this temperature range suggests that the mechanism of the reaction remains unchanged, and the rate enhancement is due to the increased molecular motion and better contact between reactants. Similar observations were reported by Vicente et al.[46] who found that transesterification rates significantly increased with temperature due to enhanced mass transfer and reduced viscosity of the reactants. However, prolonged reaction times beyond the optimal point may lead to a slight drop in conversion, potentially due to the reversible nature of transesterification or side reactions such as soap formation, as noted by Helwani et al.[47] These results reinforce the importance of optimizing reaction time, as excessive durations may not improve conversion and could negatively affect biodiesel purity due to the formation of by-products.

3.2. Catalyst characterization

TEM imaging (Fig. 2) revealed clear differences in particle morphology and dispersion among the catalysts. The unmodified CaO (Fig. 2a) displays large, densely agglomerated particles, indicating poor dispersion and limited surface area, in good agreement with BET results. The CaO–SiO$_2$ sample (Fig. 2b) exhibits a more fragmented structure, with smaller aggregated particles, suggesting that silica aids in dispersing CaO particles but still allows for some degree of agglomeration. This observation is consistent with the moderate increase in surface area and relatively lower basicity of this catalyst.

The CaO–TiO$_2$ catalyst (Fig. 2c) shows heterogeneous particle distribution with regions of finely dispersed CaO in close proximity to discrete TiO$_2$-rich domains, indicating partial segregation rather than complete uniform coating. Such morphology is consistent with wet-impregnation of TiO$_2$ (P25) followed by high-temperature calcination and suggests the coexistence of CaO, TiO$_2$, and interfacial Ca–Ti–O phases such as CaTiO$_3$. Although complete atomic-scale mixing is not observed, the presence of CaO–TiO$_2$ interfacial regions likely contributes to enhanced catalytic activity and stability, as reflected by the high BET surface area and superior FAME yield.

The CaO–Co$_2$SiO$_4$ sample demonstrates semi-uniform morphology with moderate aggregation, possibly due to the complex nature of Co$_2$SiO$_4$ formation. Although the particle distribution is less uniform than CaO–TiO$_2$, it still indicates better dispersion than unmodified CaO. Overall, TEM analysis confirms that oxide modification reduces CaO agglomeration to varying extents. In particular, partial phase segregation in the CaO–TiO$_2$ system does not hinder catalytic performance but instead appears to promote the formation of active interfacial sites, contributing to the highest observed FAME yield and apparent TOF.

Fourier-Transform infrared (FTIR) spectra of the catalysts are shown in Fig. 3a. The FTIR spectra provided for the calcium-based catalysts CaO, CaO–SiO$_2$, CaO–TiO$_2$, and CaO–Co$_2$SiO$_4$ offer significant insight into the functional groups and interactions within each sample. The FTIR spectrum of unmodified CaO shows characteristic peaks consistent with calcium

Table 2 Kinetic parameters for the FAME synthesis from waste cooking oil using CaO catalyst at different reaction temperatures

Temperature (K)	K_{app}	A ($\times 10^{-6}$ min^{-1})	E_a (kJ mol^{-1})	Y_{max} (%)^a
318	0.052	8.96	23.9	84.0
323	0.043	4.63	24.9	74.7
328	0.030	3.24	24.9	63.0
333	0.017	1.93	24.0	55.6

^{a} Maximum attainable yield FAME yield calculated from the model using the fitted parameters.
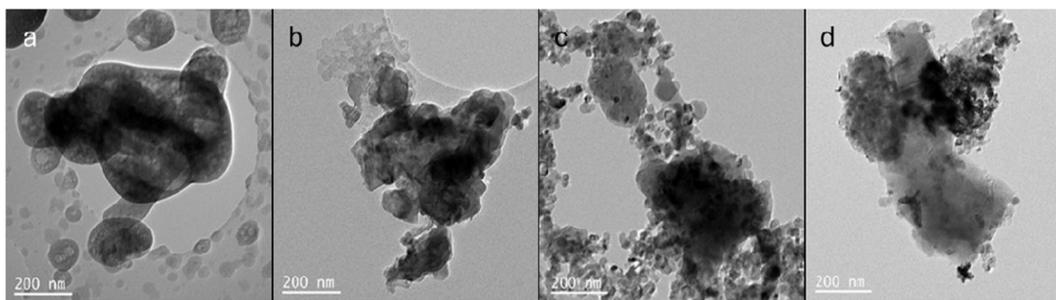
Fig. 2 TEM micrographs of (a) CaO, (b) CaO–SiO$_2$, (c) CaO–TiO$_2$ and (d) CaO–Co$_2$SiO$_4$ catalysts.

carbonate. The prominent bands observed between 1400–1500 cm^{-1} and 850–880 cm^{-1} can be assigned to the presence of carbonate (CO$_3^{2-}$) groups, likely due to the formation of calcium carbonate (CaCO$_3$) on the surface through atmospheric CO$_2$ adsorption. Additionally, the peak near 3640 cm^{-1} corresponds to the O–H stretching vibration, which can be attributed to surface hydroxyl groups or adsorbed water, a common phenomenon in CaO due to its hygroscopic nature. These carbonate and hydroxyl peaks suggest that unmodified CaO is highly reactive under ambient conditions, readily forming carbonates and hydroxyl species.

In the CaO–SiO$_2$ sample, the presence of SiO$_2$ is marked by a sharp and prominent peak around 1080 cm^{-1}, corresponding to the Si–O–Si stretching mode.[48,49] The carbonate peaks (around 1400 and 870 cm^{-1}) are still evident indicating that SiO$_2$ in the physical mixture does not affect the reactivity of CaO towards the formation of carbonates and hydroxyl. Additionally, the peak around 800 cm^{-1} may indicate the bending modes associated with Si–O–Si bonds.[19,50] The O–H peak around 3640 cm^{-1} is still present, indicating some degree of surface hydroxylation. Similarly, in the FTIR spectrum of CaO–TiO$_2$, a shoulder band at 722 cm^{-1} is indicative of Ti–O stretching, which is characteristic of anatase titanium dioxide.[22] The presence of these peaks confirms the successful incorporation of

TiO$_2$. For CaO–Co$_2$SiO$_4$, the absorption due to Co$_2$SiO$_4$ as seen at in the range of 800–1200. These bands are attributable to the Co–O–Si vibrations in cobalt orthosilicate,[51] or the Si–O–Si stretching bands. There carbonate signal in the 1400–1500 cm^{-1} range remains, possibly indicating that some carbonate species remain on the surface of the sample.

The XRD diffractograms (Fig. 3b) clearly reveal the presence of crystalline CaCO$_3$ in the CaO sample indicating that CaO reacts with atmospheric CO$_2$ to form CaCO$_3$. In the sample modified with SiO$_2$ a mixture of CaO and CaCO$_3$ is seen. However, CaCO$_3$ phase disappears completely for the samples CaO–TiO$_2$ and CaO–Ca$_2$SiO$_4$. For CaO–TiO$_2$, XRD peak which can be fitted to CaTiO$_3$ also appear at 32.3°, 48.2° and 58.3°. This structural change suggests a strong interaction between TiO$_2$ and CaO during calcination, leading to the formation of this stable mixed oxide.[21] The broadening of peaks implies a reduction in crystallinity, which could be due to the lattice distortions or defects created by the inclusion of TiO$_2$. The CaO–Co$_2$SiO$_4$ sample shows new peaks at 31.1° and 44.5°, corresponding to the formation of calcium cobalt oxide (Ca$_3$Co$_2$O$_6$).[52] This phase coexists with CaO, as the primary CaO peaks remain intact. The coexistence of these phases suggests that the incorporation of Co$_2$SiO$_4$ into the structure modifies the catalyst while maintaining the essential CaO lattice.
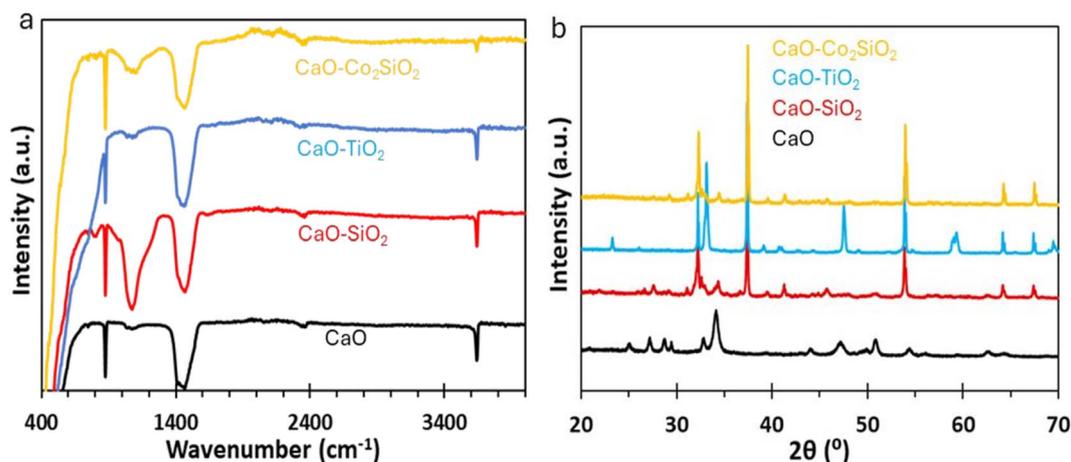

Fig. 3 (a) FTIR spectra of unmodified CaO (black), CaO–SiO$_2$ (red), CaO–TiO$_2$ (blue) and CaO–Co$_2$SiO$_4$ (yellow) catalysts prepared by PM. (b) XRD patterns of unmodified CaO (black), CaO–SiO$_2$ (red), CaO–TiO$_2$ (cyan) and CaO–Co$_2$SiO$_4$ (yellow) catalysts.

In the C 1s region of the XPS spectra (Fig. 4a–d), unmodified CaO exhibited characteristic peaks at 284.8 eV (adventitious carbon), 286.2 eV (C–O), 287.8 eV (C═O or carbonate), and 288.7 eV (CO_3^{2-}), indicating surface carbonate reformation likely due to exposure to atmospheric CO_2.[53] The CaO–TiO$_2$ sample lacked the 287.8 eV peak, suggesting suppression of carbonate or carbonyl formation by TiO$_2$, while retaining the C–O peak at 286.2 eV. This indicates that TiO$_2$ may stabilize the surface against carbonation. In contrast, CaO–SiO$_2$ and CaO–Co$_2$SiO$_4$ displayed similar carbon-related peaks to unmodified CaO, suggesting limited protection against surface contamination by these oxides. The Ca 2p spectra provided deeper insights into the chemical states of calcium (see Fig. 4e–h). Unmodified CaO and CaO–SiO$_2$ and CaO–Co$_2$SiO$_4$ all exhibited a single doublet centered at approximately 347 and 351 eV, consistent with Ca^{2+} in CaO or carbonate environments. However, CaO–TiO$_2$ showed two distinct Ca 2p doublets, indicating the presence of multiple calcium species, likely due to strong interactions between Ca and Ti leading to the formation of CaTiO$_3$. This highlights the unique role of TiO$_2$ in altering calcium's electronic environment through mixed oxide formation. These results demonstrate that oxide modifiers influence the surface chemistry and electronic properties of CaO to varying extents, with TiO$_2$ having the most pronounced effect due to its ability to integrate chemically with CaO.

3.3. Catalytic performance (effects of modification)

For the pure CaO catalyst, a basicity of 0.921 mmol g^{-1}, a surface area of 86.3 m^2 g^{-1} were determined. This surface area corresponds to a FAME yield of 80.3%, suggesting that the

activity of the catalyst is somewhat limited by its surface characteristics.[54] Incorporating SiO$_2$ into CaO increases the surface area significantly to 109.6 g m^{-2}. Despite a decrease in basicity to 0.844 mmol g^{-1}, the CaO–SiO$_2$ catalyst achieves a higher FAME yield of 84.2%. This indicates that the increased surface area provided by SiO$_2$ enhances the interaction between the catalyst and the reactants, leading to improved biodiesel production efficiency.[51] The modification of CaO with metal oxides significantly influenced FAME yield. The highest FAME yield of 89.7% was achieved with CaO–TiO$_2$, followed by CaO–Co$_2$SiO$_4$ at 87.1%. CaO–SiO$_2$ exhibited the lowest FAME yield among the modified catalysts, reaching 88.5%. Unmodified CaO had the lowest FAME yield of 80.3%, demonstrating that metal oxide modification enhances catalytic performance.

Basicity played a critical role in determining the efficiency of these catalysts. CaO–Co$_2$SiO$_4$ exhibited the highest basicity at 1.113 mmol g^{-1}, followed closely by CaO–TiO$_2$ at 1.103 mmol g^{-1}. These high basicity values correlated with the highest FAME yield, confirming the strong relationship between base strength and transesterification activity. Modified catalysts showed similar trends, with CaO–TiO$_2$ and CaO–Co$_2$SiO$_4$ having higher basicity and FAME yield compared to CaO–SiO$_2$. The lower basicity of CaO–SiO$_2$ at 0.832 mmol g^{-1} contributed to its reduced catalytic efficiency despite its high surface area. Since transesterification is a base-catalyzed reaction, catalysts with stronger basic sites generally exhibit higher biodiesel yields.[54]

Surface area also influenced oil conversion, though its effect was secondary to basicity. CaO–TiO$_2$ and CaO–SiO$_2$ exhibited the highest surface areas of 121.9 m^2 g^{-1} and 119.3 m^2 g^{-1}, respectively, whereas CaO–Co$_2$SiO$_4$ had a lower surface area of 98.4 m^2 g^{-1}. Despite this, CaO–Co$_2$SiO$_4$ outperformed CaO–SiO$_2$
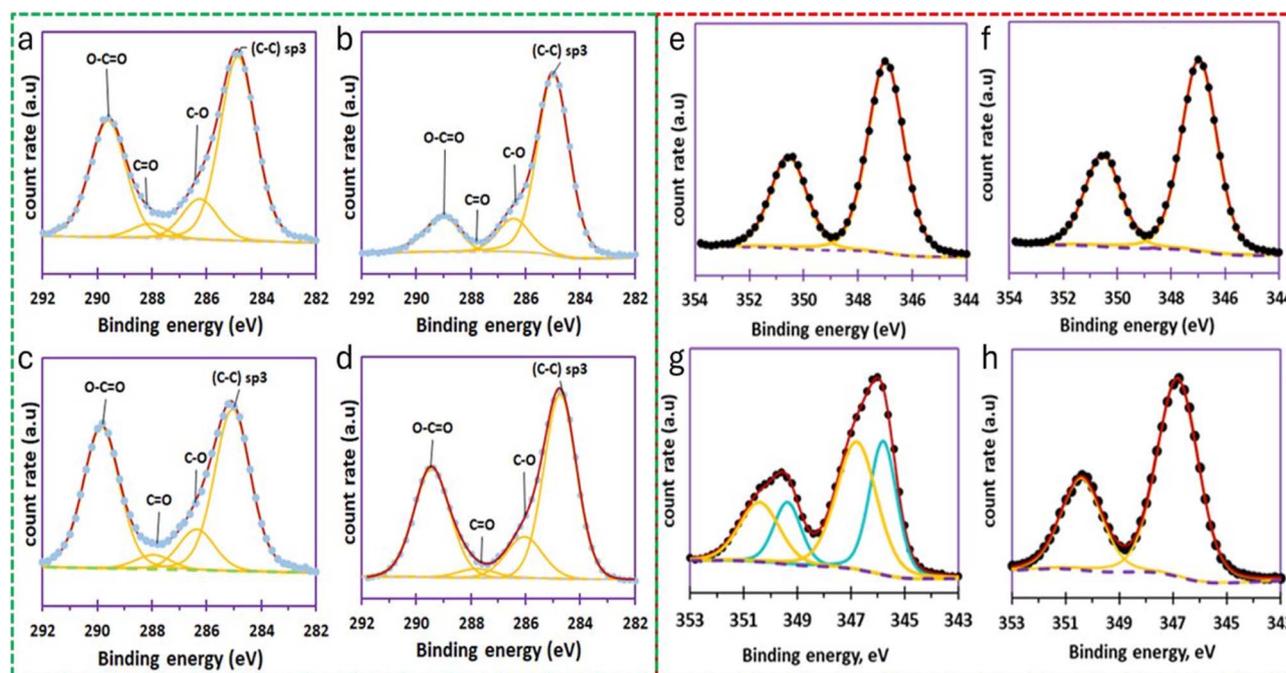

Fig. 4 C 1s X-ray photoemission profiles of (a) CaO, (b) CaO−SiO$_2$, (c) CaO−TiO$_2$ and (d) CaO−Co$_2$SiO$_4$ and Ca 2p X-ray photoemission profiles of (e) CaO, (f) CaO−SiO$_2$, (g) CaO−TiO$_2$ and (h) CaO−Co$_2$SiO$_4$.

in oil conversion, reinforcing that basicity plays a more dominant role than surface area in catalytic efficiency. Among the modified catalysts, CaO–SiO$_2$ exhibited a higher surface area than CaO–Co$_2$SiO$_4$ but had a lower conversion, supporting the notion that an optimal balance between basicity and surface area is necessary for maximizing biodiesel yield.[55] Unmodified CaO exhibited the lowest FAME yield, which can be attributed to its lower basicity of 0.921 mmol g^{-1} and smaller surface area of 86.3 m^2 g^{-1}. The presence of CaCO$_3$ in unmodified CaO likely reduced the number of active basic sites, further limiting its catalytic efficiency. These findings indicate that modification not only improves catalyst performance but also stabilizes basic sites, reducing deactivation caused by carbonation.[17]

The impact of modification on FAME yield highlights the need to optimize both basicity and surface area for maximum catalytic efficiency. Overall, the data in Table 3 highlights the importance of optimizing both basicity and surface area to achieve high biodiesel yield. TiO$_2$ modification emerged as the most effective, followed by Co$_2$SiO$_4$, while SiO$_2$ modification, despite enhancing surface area, had a lower impact on biodiesel yield due to its weaker basicity. The superiority of the impregnation method over physical mixing further reinforces the importance of preparation techniques in catalyst design. These findings contribute to the development of highly efficient and stable heterogeneous catalysts for biodiesel synthesis, with potential applications in sustainable biofuel production.[55]

To enable a site-normalized comparison of catalytic activity, apparent turnover frequencies (TOFs) were calculated from the GC-derived fatty acid methyl ester (FAME) yield after 60 minutes under optimized reaction conditions, using the measured basicity values and catalyst mass employed. These TOFs are described as apparent because they were determined at relatively high conversions under batch conditions, where approach to equilibrium, evolving reactant concentrations, and time-dependent changes in site availability (e.g., leaching or surface carbonation) may influence the observed rates. Accordingly, TOF values are interpreted as operational performance indicators rather than intrinsic kinetic constants.

When normalized by basic site concentration, the catalysts exhibit broadly comparable per-site activities, indicating that oxide modification primarily influences the number, accessibility, and stability of basic sites rather than dramatically altering intrinsic site activity. Minor differences in apparent TOF among the catalysts may reflect variations in site accessibility and dispersion. In contrast, the higher overall FAME yields observed for TiO$_2$- and Co$_2$SiO$_4$-modified CaO are

attributed mainly to increased total basicity and improved catalyst stability rather than a substantial enhancement in intrinsic per-site reaction rates.

Equilibrium modelling of FAME production: cooperative adsorption *via* the Hill Isotherm to investigate the effect of the alcohol-to-oil ratio on transesterification equilibrium, FAME yield was measured at varying initial methanol-to-oil molar ratios ($Q_i = 4 : 1$ to $14 : 1$). FAME yield with Q_i, peaking at 89.7% at a ratio of $10 : 1$ before declining, suggesting an optimal stoichiometric balance. The equilibrium final ratio Q_f was calculated as:

$$Q_f = \frac{Q_i - 3x}{1 - x}$$

where x is the fractional oil conversion. This calculation assumes a stoichiometric factor of 3, corresponding to the transesterification of pure triglycerides. Waste cooking oil (WCO), however, contains free fatty acids, mono- and diglycerides, and minor impurities, which may alter the effective methanol requirement. Therefore, Q should be interpreted as an apparent equilibrium ratio rather than the exact stoichiometric ratio for all reactive species. Remarkably, all catalysts—regardless of composition—followed a single equilibrium trend when FAME yield was plotted against Q_f (Fig. 5). This indicates that while catalyst modifications influence reaction kinetics, they do not affect the thermodynamic equilibrium of the system.
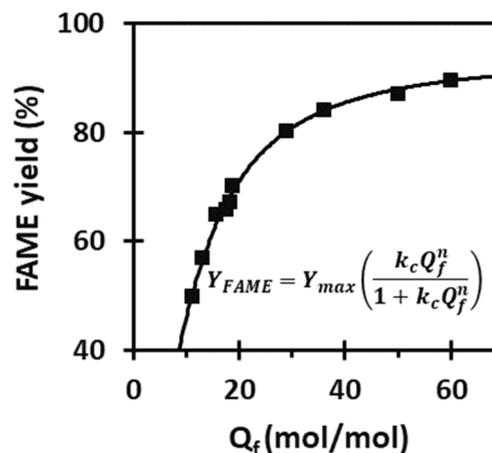

$$Y_{FAME} = Y_{max}\left(\frac{k_c Q_f^n}{1 + k_c Q_f^n}\right)$$

Fig. 5 FAME yield as a function of the final MeOH-to-oil ratio in solution.

Table 3 Comparison of basicity, surface area, and FAME yield for various CaO-based catalysts (methanol-to-oil ratio = 10 : 1, 333 K, 5% w/v, 60 minutes duration)

	Catalyst basicity (mmol g^{-1})	Surface area (m^2 g^{-1})	FAME yield (%)	Apparent TOF (s^{-1})
CaO	0.921	86.3	80.3	0.0059
Cao–SiO$_2$	0.832	119.3	84.2	0.0067
CaO–TiO$_2$	1.103	121.9	89.7	0.0056
CaO–Co$_2$SiO$_4$	1.113	98.4	87.1	0.0053

The equilibrium data were modeled using the Hill isotherm, a framework traditionally applied to cooperative binding in biochemical systems but here employed as a phenomenological saturation model in heterogeneous biodiesel catalysis. The model is expressed as the Hill equation:

$$Y_{FAME} = Y_{max}\left(\frac{k_c Q_f{}^n}{1 + k_c Q_f{}^n}\right)$$

where Y_{FAME} is the fractional FAME yield, Y_{max} is the maximum attainable FAME yield under the investigated conditions, Q_f is the methanol-to-oil molar ratio, k_c is an apparent equilibrium constant reflecting the effectiveness of methanol excess, and n is the Hill coefficient. The Hill coefficient is treated here as a phenomenological descriptor of non-linear saturation behaviour rather than as evidence of molecular cooperativity. Model parameters were obtained by non-linear regression and are shown in Table 4.

The fitting yielded a Hill coefficient ($n = 1.7 \pm 0.1$) and an equilibrium constant (0.019 ± 0.003), indicating a non-linear, sigmoidal dependence of FAME yield on methanol-to-oil ratio rather than true molecular cooperativity. In this context, the Hill coefficient is interpreted as an apparent descriptor of saturation behavior, reflecting surface heterogeneity, competitive adsorption, and equilibrium constraints, rather than cooperative binding in the biochemical sense. The universal collapse of all catalyst data onto a single Hill isotherm suggests that this non-linear saturation behavior is governed primarily by reaction thermodynamics and phase equilibrium effects, rather than being a strictly catalyst-specific adsorption phenomenon. To assess the thermodynamics of adsorption, the standard Gibbs free energy change (ΔG°) was calculated from the equilibrium constant K derived from the Hill model using the relation:

$$\Delta G^\circ = -RT \ln K$$

where R is the universal gas constant and T is the absolute temperature in Kelvin. The positive ΔG° value (+10.8 kJ mol^{-1} at 333 K) indicates that adsorption is slightly non-spontaneous under the experimental conditions, consistent with the low equilibrium constant. The excellent fit of the Hill isotherm to the equilibrium data ($R^2 > 0.98$) and the observation of a Hill coefficient greater than one highlight a universal cooperative adsorption mechanism governing the system's thermodynamics. Although catalyst modifiers such as TiO$_2$, Co$_2$SiO$_4$, and SiO$_2$ impact reaction rates and kinetics, they do not significantly alter the fundamental adsorption equilibrium. This understanding reveals an underexplored dimension in catalyst design: engineering catalysts to enhance cooperative adsorption interactions can potentially improve catalytic efficiency. This insight is especially valuable for developing robust catalysts tailored to waste-derived feedstocks, where catalyst stability and reusability are critical.

3.4. Durability tests

To assess the reusability of the catalysts, a rigorous testing procedure was followed. After each reaction cycle, the catalysts were carefully recovered by filtration, washed thoroughly with n-hexane to remove residual reactants or products, and then dried and calcined at 573 K to restore their catalytic activity. Remarkably, more than 90% of the catalyst mass was successfully recovered after each cycle. The mass loss was compensated by adjusting the reaction volume to maintain a constant catalyst loading of 5%. The change in reaction volume was insignificant, as the recovery rate ranged from 90% to 94% per cycle. The performance of pure CaO declined steadily with each reuse, showing a noticeable decrease in catalytic activity from the first cycle onwards (Fig. 6). The total activity loss after four cycles was 7.5%, which can be attributed to the degradation of the CaO structure, leaching of active sites, and the potential formation of calcium glyceroxide that can block catalytic sites and inhibit further reactions.[56,57] This structural deterioration ultimately reduces the basicity and surface area essential for efficient biodiesel production. In contrast, CaO-based catalysts modified with SiO$_2$, TiO$_2$, and Co$_2$SiO$_4$ exhibited much better reusability. After four reaction cycles, the activity loss for CaO–SiO$_2$, CaO–TiO$_2$, and CaO–Co$_2$SiO$_4$ was only 2.3%, 1.1%, and 0.7%, respectively. The decline in catalytic activity for these catalysts

Table 4 Modelling the equilibrium parameters of the FAME production

Parameter	Value
K, mM^{-n}	0.019 ± 0.003
N	1.7 ± 0.1
$^a Y_{max}$ (%)	94.0 ± 0.8
ΔG° (kJ mol^{-1})	10.8

^{a} $Y_{FAME} = Y_{max}\left(\dfrac{k_c Q_f{}^n}{1 + k_c Q_f{}^n}\right)$.

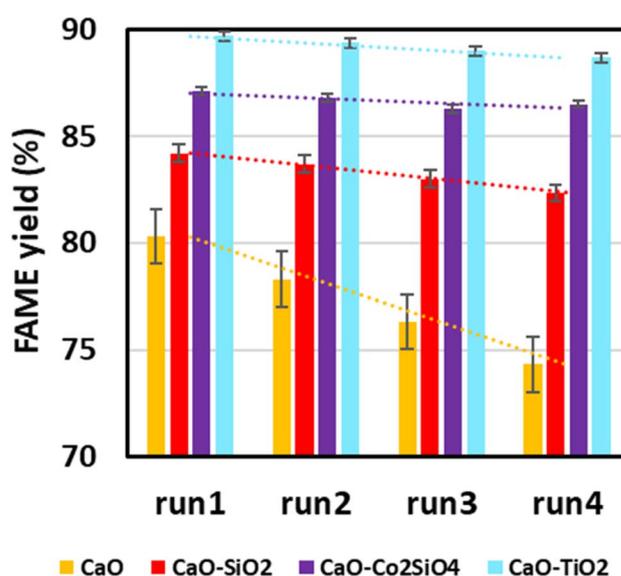**Fig. 6** Catalyst reusability over four transesterification cycles using (yellow) unmodified CaO, (red) CaO–SiO$_2$, (purple) CaO–TiO$_2$, and (pink) CaO–Co$_2$SiO$_4$.

only became apparent after four cycles, highlighting their superior stability compared to pure CaO. The improved durability is attributed to the stabilizing effect of the oxide supports, which prevent severe structural degradation and limit the leaching of active CaO species.[58] Moreover, the chemical interaction between CaO and the supports (especially in the impregnated samples) leads to stronger phase adhesion, enhanced thermal stability, and better retention of basic active sites. This enhanced reusability makes CaO-based mixed oxide catalysts more suitable for sustainable and cost-effective biodiesel production processes.

4. Conclusions

This study demonstrated how targeted oxide modification can significantly enhance the catalytic performance of waste eggshell-derived CaO for biodiesel production from waste cooking oil. Systematic comparison of SiO_2-, TiO_2-, and Co_2SiO_4-modified CaO revealed distinct structure–function relationships. TiO_2 modification yielded the highest FAME yield (89.7%) driven by synergistic increases in basicity and surface area and supported by the formation of a $CaTiO_3$ phase. Co_2SiO_4, applied here for the first time in biodiesel catalysis, imparted exceptional stability, retaining over 99% activity after four cycles, while SiO_2 served as a benchmark oxide, enhancing dispersion without major alteration of surface chemistry. Equilibrium modelling using the Hill isotherm provided new insight into cooperative adsorption phenomena in biodiesel catalysis, with TiO_2- and Co_2SiO_4-modified CaO exhibiting positive cooperativity ($n > 1$) — a feature rarely reported in this context. These findings indicate that surface modification not only improves yield and durability but can also tailor the adsorption behaviour of active sites to enhance catalytic efficiency. By integrating waste valorization, applied catalytic testing, and mechanistic modelling, this work presents a scalable, low-cost route to durable heterogeneous catalysts for sustainable biodiesel production. The combination of performance optimization with cooperative adsorption insights offers a foundation for future designs of waste-derived catalysts with improved site synergy, stability, and economic viability.

Conflicts of interest

There are no conflicts to declare.

Data availability

All data supporting the findings of this study are contained within the manuscript.

Acknowledgements

References

1 F. Perera, Pollution from Fossil-Fuel Combustion Is the Leading Environmental Threat to Global Pediatric Health and Equity: Solutions Exist, *Int. J. Environ. Res. Public Health*, 2018, **15**, 16–32, DOI: 10.3390/ijerph15010016.

2 N. Ghosh, D. Rhithuparna, S. L. Rokhum and G. Halder, Ethical Issues Pertaining to Sustainable Biodiesel Synthesis over Trans/Esterification Process, *Sustainable Chem. Pharm.*, 2023, **33**, 101123, DOI: 10.1016/j.scp.2023.101123.

3 R. El-Araby, Biofuel Production: Exploring Renewable Energy Solutions for a Greener Future, *Biotechnol. Biofuels Bioprod.*, 2024, **17**(1), 129, DOI: 10.1186/s13068-024-02571-9.

4 B. Panchal, C. H. Su, C. C. Fu, S. J. Wu and H. Y. Juan, Ecofriendly and Cost-Effective Biodiesel Production from Water Containing Feedstocks through Electrolysis-a Review, *Fuel Process. Technol.*, 2025, **276**, 108277, DOI: 10.1016/j.fuproc.2025.108277.

5 S. F. Basumatary, S. Brahma, M. Hoque, B. K. Das, M. Selvaraj, S. Brahma and S. Basumatary, Advances in CaO-Based Catalysts for Sustainable Biodiesel Synthesis, *Green Energy Resour.*, 2023, **1**(3), 100032, DOI: 10.1016/j.gerr.2023.100032.

6 K. Liu, L. Zhang, G. Wei, Y. Yuan and Z. Huang, Synthesis, Characterization and Application of a Novel Carbon-Doped Mix Metal Oxide Catalyst for Production of Castor Oil Biodiesel, *J. Cleaner Prod.*, 2022, **373**, 133768, DOI: 10.1016/j.jclepro.2022.133768.

7 A. Arumugam and P. Sankaranarayanan, Biodiesel Production and Parameter Optimization: An Approach to Utilize Residual Ash from Sugarcane Leaf, a Novel Heterogeneous Catalyst, from Calophyllum Inophyllum Oil, *Renewable Energy*, 2020, **153**, 1272–1282, DOI: 10.1016/j.renene.2020.02.101.

8 F. Yaşar, Comparison of Fuel Properties of Biodiesel Fuels Produced from Different Oils to Determine the Most Suitable Feedstock Type, *Fuel*, 2020, **264**, 116817, DOI: 10.1016/j.fuel.2019.116817.

9 S. Sankhyan, P. Kumar, S. Pandit and S. Ray, Valorization of Waste Cooking Oil: Emerging Strategies for Bio-Based Product Development, *Biomass Bioenergy*, 2025, **202**, 108244, DOI: 10.1016/j.biombioe.2025.108244.

10 L. S. Al-Saadi, V. C. Eze and A. P. Harvey, Techno-Economic Analysis of Processes for Biodiesel Production with Integrated Co-Production of Higher Added Value Products from Glycerol, *Biofuels*, 2022, **13**(4), 489–496, DOI: 10.1080/17597269.2020.1767495.

11 G. M. Figueroa-Torres and C. Theodoropoulos, Techno-Economic Analysis of a Microalgae-Based Biorefinery Network for Biofuels and Value-Added Products, *Bioresour. Technol. Rep.*, 2023, **23**, 101524, DOI: 10.1016/j.biteb.2023.101524.

12 L. Macheli, M. E. Malefane and L. L. Jewell, Waste-Derived Calcium Oxide Catalysts in Biodiesel Production: Exploring

Various Waste Sources, Deactivation Challenges, and Improvement Strategies, *Bioresour. Technol. Rep.*, 2025, **29**, 102021, DOI: 10.1016/j.biteb.2025.102021.

13 T. A. Degfie, T. T. Mamo and Y. S. Mekonnen, Optimized Biodiesel Production from Waste Cooking Oil (WCO) Using Calcium Oxide (CaO) Nano-Catalyst, *Sci. Rep.*, 2019, **9**(1), 1–8, DOI: 10.1038/s41598-019-55403-4.

14 B. Basumatary, B. Das, B. Nath and S. Basumatary, Current Research in Green and Sustainable Chemistry Synthesis and Characterization of Heterogeneous Catalyst from Sugarcane Bagasse : Production of Jatropha Seed Oil Methyl Esters, *Curr. Res. Green Sustainable Chem.*, 2021, **4**, 100082, DOI: 10.1016/j.crgsc.2021.100082.

15 B. Nath, B. Basumatary, S. Brahma, B. Das and P. Kalita, Musa Champa Peduncle Waste-Derived Efficient Catalyst : Studies of Biodiesel Synthesis , Reaction Kinetics and Thermodynamics, *Energy*, 2023, **270**, 126976, DOI: 10.1016/j.energy.2023.126976.

16 Y. S. Erchamo, T. T. Mamo, G. A. Workneh and Y. S. Mekonnen, Improved Biodiesel Production from Waste Cooking Oil with Mixed Methanol–Ethanol Using Enhanced Eggshell-Derived CaO Nano-Catalyst, *Sci. Rep.*, 2021, **11**(1), 1–12, DOI: 10.1038/s41598-021-86062-z.

17 M. Mohamad, N. Ngadi, S. Wong, N. Y. Yahya, I. M. Inuwa and N. S. Lani, Synthesis and Characterization of CaO-TiO2 for Transesterification of Vegetable Palm Oil, *Int. J. Eng., Trans. B*, 2018, **31**(8), 1326–1333, DOI: 10.5829/ije.2018.31.08b.22.

18 M. Sharifi, S. Tangestaninejad, M. Moghadam and A. Marandi, CaO/ZnO Composites as Stable Catalysts for Biodiesel Production from Soybean Oil at Room Temperature, *Sci. Rep.*, 2025, **15**, 3610–3622.

19 L. Macheli, G. M. Leteba, B. P. Doyle, L. Jewell and E. van Steen, Modulating CO Hydrogenation Activity through Silane Functionalization of Cobalt Catalysts, *Appl. Catal., A*, 2024, **685**(May), 119874, DOI: 10.1016/j.apcata.2024.119874.

20 X. J. Yin, K. Peng, A. P. Hu, L. P. Zhou, J. H. Chen and Y. W. Du, Preparation and Characterization of Core-Shell Structured Co/SiO2nanosphere, *J. Alloys Compd.*, 2009, **479**(1–2), 372–375, DOI: 10.1016/j.jallcom.2008.12.070.

21 J. M. Luque-Centeno, M. V. Martínez-Huerta, D. Sebastián, J. I. Pardo and M. J. Lázaro, CoTiO3/NrGO Nanocomposites for Oxygen Evolution and Oxygen Reduction Reactions: Synthesis and Electrocatalytic Performance, *Electrochim. Acta*, 2020, **331**, 135396, DOI: 10.1016/j.electacta.2019.135396.

22 B. Čolović, D. Kisić, B. Jokanović, Z. Rakočević, I. Nasov, A. T. Petkoska and V. Jokanović, Wetting Properties of Titanium Oxides, Oxynitrides and Nitrides Obtained by DC and Pulsed Magnetron Sputtering and Cathodic Arc Evaporation, *Mater. Sci.-Pol.*, 2019, **37**(2), 173–181, DOI: 10.2478/msp-2019-0031.

23 S. I. Hansen, B. H. Sjølin, I. E. Castelli, T. Vegge, A. D. Jensen and J. M. Christensen, An Adsorption Isotherm That Includes the Interactions between Adsorbates, *J. Phys. Chem. C*, 2025, **129**, 5393–5407, DOI: 10.1021/acs.jpcc.4c08754.

24 N. Ghosh, D. Rhithuparna, S. L. Rokhum and G. Halder, Evaluating the Scale-Up Potential of Biogenic Heterogeneous Catalyst for Biodiesel Production, *ACS Sustainable Resour. Manage.*, 2024, **1**(3), 480–492, DOI: 10.1021/acssusresmgt.3c00111.

25 S. Sirisomboonchai, M. Abuduwayiti, G. Guan, C. Samart, S. Abliz, X. Hao, K. Kusakabe and A. Abudula, Biodiesel Production from Waste Cooking Oil Using Calcined Scallop Shell as Catalyst, *Energy Convers. Manage.*, 2015, **95**, 242–247, DOI: 10.1016/j.enconman.2015.02.044.

26 K. Tanabe and T. Yamaguchi, Instructions for Use BASICITY AND ACIDITY OF SOLID SURFACES, *J. Res. Inst. Catal., Hokkaido Univ.*, 1963, **11**(3), 179–184.

27 K. R. Iyer and A. Bhan, Particle Size Dependence of Ethylene Epoxidation Rates on Ag/α-Al2O3 Catalysts: Why Particle Size Distributions Matter, *J. Catal.*, 2023, **420**, 99–109, DOI: 10.1016/j.jcat.2023.02.008.

28 I. F. Ejim and F. Kamen, Physiochemical Characterization of Algae Oil from Microalgae of Nike Lake Enugu, *J. Eng. Appl. Sci.*, 2013, **5**(1), 181–187.

29 M. I. Atadashi, The Effects of Alcohol to Oil Molar Ratios and the Type of Alcohol on Biodiesel Production Using Transesterification Process, *Egypt. J. Pet.*, 2016, **25**(1), 21–31, DOI: 10.1016/j.ejpe.2015.06.007.

30 I. M. Atadashi, M. K. Aroua and A. A. Aziz, Biodiesel Separation and Purification: A Review, *Renewable Energy*, 2011, **36**(2), 437–443, DOI: 10.1016/j.renene.2010.07.019.

31 H. Hamze, M. Akia and F. Yazdani, Optimization of Biodiesel Production from the Waste Cooking Oil Using Response Surface Methodology, *Process Saf. Environ. Prot.*, 2015, **94**(C), 1–10, DOI: 10.1016/j.psep.2014.12.005.

32 A. C. Gumahin, J. M. Galamiton, M. J. Allerite, R. S. Valmorida, J. R. L. Laranang, V. I. F. Mabayo, R. O. Arazo and A. L. Ido, Response Surface Optimization of Biodiesel Yield from Pre-Treated Waste Oil of Rendered Pork from a Food Processing Industry, *Bioresour. Bioprocess.*, 2019, **6**, 48–60, DOI: 10.1186/s40643-019-0284-2.

33 W. Bajwa, A. Ikram, M. A. I. Malik, L. Razzaq, A. R. Khan, A. Latif, F. Hussain and A. Qazi, Optimization of Biodiesel Yield from Waste Cooking Oil and Sesame Oil Using RSM and ANN Techniques, *Heliyon*, 2024, **10**(15), e34804, DOI: 10.1016/j.heliyon.2024.e34804.

34 V. Mandari and S. K. Devarai, Biodiesel Production Using Homogeneous, Heterogeneous, and Enzyme Catalysts via Transesterification and Esterification Reactions: A Critical Review, *Bioenergy Res.*, 2022, **15**(2), 935–961, DOI: 10.1007/s12155-021-10333-w.

35 W. Limmun, T. Chungcharoen, C. Rattanamechaiskul, K. Phetpan and W. Limmun, Enhancing Biodiesel Yield and Purification with a Recently Developed Centrifuge Machine: A Response Surface Methodology Approach, *Heliyon*, 2024, **10**(7), e29018, DOI: 10.1016/j.heliyon.2024.e29018.

36 F. Mirshafiee and M. Rezaei, Optimizing Al/Zn Ratios in K2O/Zn-Aluminate Catalysts for Enhanced Biodiesel Production Efficiency, *Sci. Rep.*, 2025, **15**, 25293–25306, DOI: 10.1038/s41598-025-11268-4.

37 M. Yaghi, S. Chidiac, S. Awad, Y. El Rayess and N. Zgheib, An Overview of Biodiesel Production via Heterogeneous Catalysts: Synthesis, Current Advances, and Challenges, *Clean Technol.*, 2025, **7**(3), 62, DOI: 10.3390/cleantechnol7030062.

38 W. M. Kedir, K. T. Wondimu and G. S. Weldegrum, Optimization and Characterization of Biodiesel from Waste Cooking Oil Using Modified CaO Catalyst Derived from Snail Shell, *Heliyon*, 2023, **9**(5), e16475, DOI: 10.1016/j.heliyon.2023.e16475.

39 I. de Araújo Sobrinho, T. S. Ribeiro, A. C. Dias e Silva, M. Arrais Gonçalves, G. N. d. Rocha Filho and L. R. Vieira da Conceição, Catalytic Solid Derived from Residual Bean Husk Biomass Applied to Sustainable Biodiesel Production: Preparation, Characterization, and Regeneration Study, *RSC Adv.*, 2025, **15**(9), 7050–7068, DOI: 10.1039/d5ra01195g.

40 K. T. T. Amesho, Y. C. Lin, C. E. Chen, P. C. Cheng and V. K. Ponnusamy, Optimization and Kinetics Studies of Biodiesel Synthesis from Jatropha Curcas Oil under the Application of Eco-Friendly Microwave Heating Technique: An Environmentally Benign and Sustainable Bio-Waste Management Approach, *Sustainable Environ. Res.*, 2022, **32**, 41–53, DOI: 10.1186/s42834-022-00151-w.

41 S. M. Yahya, M. Danish, A. Ahmed, A. Equbal, Z. A. Khan and M. Asjad, RSM Based Optimization of Process Parameters of Biodiesel Production from Waste Palm Oil Using Modified Nano-Catalyst, *npj Clean Energy*, 2025, **1**(1), 1–14, DOI: 10.1038/s44406-024-00001-1.

42 L. C. Meher, D. Vidya Sagar and S. N. Naik, Technical Aspects of Biodiesel Production by Transesterification - A Review, *Renewable Sustainable Energy Rev.*, 2006, **10**(3), 248–268, DOI: 10.1016/j.rser.2004.09.002.

43 V. H. Carvalho-Silva, N. D. Coutinho and V. Aquilanti, Temperature Dependence of Rate Processes beyond Arrhenius and Eyring: Activation and Transitivity, *Front. Chem.*, 2019, **7**, 1–11, DOI: 10.3389/fchem.2019.00380.

44 N. Salahudeen and A. A. Rasheed, Kinetics and Thermodynamics of Hydrolysis of Crystal Violet at Ambient and below Ambient Temperatures, *Sci. Rep.*, 2020, **10**(1), 1–9, DOI: 10.1038/s41598-020-78937-4.

45 A. S. Silitonga, H. H. Masjuki, H. C. Ong, T. Yusaf, F. Kusumo and T. M. I. Mahlia, Synthesis and Optimization of Hevea Brasiliensis and Ricinus Communis as Feedstock for Biodiesel Production: A Comparative Study, *Ind. Crops Prod.*, 2016, **85**, 274–286, DOI: 10.1016/j.indcrop.2016.03.017.

46 G. Vicente, M. Martínez and J. Aracil, Integrated Biodiesel Production: A Comparison of Different Homogeneous Catalysts Systems, *Bioresour. Technol.*, 2004, **92**(3), 297–305, DOI: 10.1016/j.biortech.2003.08.014.

47 Z. Helwani, M. R. Othman, N. Aziz, J. Kim and W. J. N. Fernando, Solid Heterogeneous Catalysts for Transesterification of Triglycerides with Methanol: A Review, *Appl. Catal., A*, 2009, **363**(1–2), 1–10, DOI: 10.1016/j.apcata.2009.05.021.

48 D. G. Kurth and T. Bein, Thin-Films of (3-Aminopropyl) Triethoxysilane on Aluminum-Oxide and Gold Substrates, *Langmuir*, 1995, **11**(8), 3061–3067, DOI: 10.1021/la00008a035.

49 X. Huang and Z. Chen, Preparation of CoFe2O4/SiO2nanocomposites by Sol-Gel Method, *J. Cryst. Growth*, 2004, **271**(1–2), 287–293, DOI: 10.1016/j.jcrysgro.2004.07.064.

50 A. P. Kafle, D. McKeown, W. Wong-Ng, M. Alsubaie, M. Alenezi, I. L. Pegg and B. Dutta, Raman Spectroscopy and Electrical Transport in 30Li2O● (67−x) B2O3●(x) SiO2●3Al2O3 Glasses, *Electron. Mater.*, 2024, **5**(3), 166–188, DOI: 10.3390/electronicmat5030012.

51 S.-J. Jong and S. Cheng, Reduction Behavior and Catalytic Properties of Cobalt Containing ZSM-5 Zeolites, *Appl. Catal., A*, 1995, **126**(1), 51–66, DOI: 10.1016/0926-860X(95)00016-X.

52 S. Kahatta, N. Chaiyo, C. Ruttanapun, W. Techitdheera, W. Pecharapa and N. Vittayakorn, Microwave-Assisted Solution Combustion Synthesis and Characterization of Thermoelectric, *Adv. Mater. Res.*, 2013, **802**, 84–88, DOI: 10.4028/www.scientific.net/AMR.802.84.

53 L. H. Grey, H. Y. Nie and M. C. Biesinger, Defining the Nature of Adventitious Carbon and Improving Its Merit as a Charge Correction Reference for XPS, *Appl. Surf. Sci.*, 2024, **653**, 159319, DOI: 10.1016/j.apsusc.2024.159319.

54 R. Alsaiari, E. Musa and M. Rizk, Effects of Calcination Temperature of Eggshell-Derived CaO as a Catalyst for Biodiesel Production from Waste Cooking Oil, *S. Afr. J. Chem.*, 2023, **77**, 30–35, DOI: 10.17159/0379-4350/2023/v77a05.

55 R. Manurung, S. Z. D. M. Parinduri, R. Hasibuan, B. H. Tarigan and A. G. A. Siregar, Synthesis of Nano-CaO Catalyst with SiO2 Matrix Based on Palm Shell Ash as Catalyst Support for One Cycle Developed in the Palm Biodiesel Process, *Case Stud. Chem. Environ. Eng.*, 2023, **7**, 100345, DOI: 10.1016/j.cscee.2023.100345.

56 J. Boro, D. Deka and A. J. Thakur, A Review on Solid Oxide Derived from Waste Shells as Catalyst for Biodiesel Production, *Renewable Sustainable Energy Rev.*, 2012, **16**(1), 904–910, DOI: 10.1016/j.rser.2011.09.011.

57 M. Kouzu and J. S. Hidaka, Transesterification of Vegetable Oil into Biodiesel Catalyzed by CaO: A Review, *Fuel*, 2012, **93**, 1–12, DOI: 10.1016/j.fuel.2011.09.015.

58 X. Liu, H. He, Y. Wang, S. Zhu and X. Piao, Transesterification of Soybean Oil to Biodiesel Using CaO as a Solid Base Catalyst, *Fuel*, 2008, **87**(2), 216–221, DOI: 10.1016/j.fuel.2007.04.013.